Hindawi
Journal of Chemistry
Volume 2023, Article ID 6677710, 15 pages
https://doi.org/10.1155/2023/6677710

Research Article

Fixed-Bed Adsorption of an Azo Dye (Methyl Orange) onto Chemically and Thermally Regenerated Activated Carbons

Idriss Kamdem Taquieteu,[1] Hermann Tamaguelon Dzoujo,[1] Victor Odhiambo Shikuku,[2] Charles Banenzoué,[1] and Daniel David Joh Dina[1]

[1]*Department of Chemistry, Faculty of Sciences, University of Douala, P.O. Box 24157, Douala, Cameroon*
[2]*Department of Physical Sciences, Kaimosi Friends University, P.O. Box 385-50309, Kaimosi, Kenya*

Correspondence should be addressed to Hermann Tamaguelon Dzoujo; hermann.dzoujo@gmail.com and Daniel David Joh Dina; dinadavidcr@yahoo.com

Received 9 August 2023; Revised 23 November 2023; Accepted 2 December 2023; Published 15 December 2023

Academic Editor: Kokhwa Lim

In this study, the effectiveness of the recovery method for spent granular activated carbon (SGAC) for application in dye removal was evaluated. A comparative study of the textural (porosity), compositional, surface functionality, and adsorption performance of chemically (CAR400) and thermally regenerated activated carbons (CAR700 and CAR900) was conducted for the elimination of methyl orange (MO) dye by using a fixed-bed system. The results were compared with those of commercial activated carbon (CA). The influence of parameters such as the initial dye concentration, the flow rate, the internal diameter of the column, and the bed height was evaluated. Adsorption data were modelled by using the Thomas, Adams–Bohart, and Yoon–Nelson equations. The CAR400 activated carbon had a microporosity (1045 mg/g) comparable to that of the reference commercial (CA) activated carbon (1052 mg/g) but exhibited the least adsorption capacity. The breakthrough curves were best described by the Thomas model more than the Bohart–Adams and Yoon–Nelson's models. Thomas's model depicted that an increase in column diameter resulted in a decrease in the maximum adsorption capacity (q_o). The CAR900 material exhibited the highest adsorption capacity (15.72 mg/g) comparable to that of commercial activated carbon, CA (16.90 mg/g). These results show that the physical/thermal regeneration of spent granular activated carbons (SGAC) is more suitable for the valorization of these waste materials for water purification applications.

1. Introduction

Millions of tons of chemicals are manufactured worldwide each year, and from their synthesis to their use, they generate wastes with suspended solids and dissolved substances, which can disrupt the natural balance and thus become a major source of contamination of soil, surface water, and groundwater [1]. All industrial cities in the world face these pollution problems, and Douala (Cameroon) is not an isolated case. The pollutants, mostly organic, include detergents, pesticides, and concentrated dyes from the textile industry. The textile industry is the most polluting and water-consuming sector, generating highly toxic wastewater due to the presence of several colourants and other chemical compounds [2]. These dyes are not easily biodegradable, and the colouration is visible even at relatively low concentrations (below 1 mg/L) [3, 4]. The impact of these dye-containing effluents, which are overly coloured, with highly variable pH values and high chemical oxygen demand (COD) on the ecosystem are severely felt by the fauna and flora in the recipient water bodies [5]. Regarding pollution control standards, the permissible levels of the various pollutants discharged by industries into the environment are set at lower levels, and for drinking water, the limit for azo dyes is set at 3.1 $\mu g \cdot L^{-1}$ according to DEPA (Danish Environmental Protection Agency). It is becoming imperative for relevant industries to implement simple and inexpensive processes capable of meeting these stringent requirements.

Some of the methods for treating and decolorizing polluted effluents include coagulation, flocculation, biodegradation, membrane filtration, chemical oxidation, ozonation, ion exchange, electrochemical methods, and adsorption [6]. Of these processes, the adsorption method is still the most widely used method for dye removal due to its efficiency, inexpensiveness, and simplicity, the main criteria for the selection of adsorbing materials [7]. Several materials such as clays, zeolites, activated alumina, silica gels, geopolymer, and activated carbons have been evaluated for water treatment and decolourization process [8, 9]. Methyl orange (MO), a sulfonated azo dye, is recalcitrant to traditional wastewater treatment approaches due to its functional groups [10]. Furthermore, dyes containing aromatic amines in their chemical structures, such as MO, are known to be carcinogenic owing to the production of benzidine compounds through biotransformation [11]. Removal of MO from wastewater is therefore critical. Several adsorbents have been reported for the removal of methyl orange from water. Khelifi et al. [12] reported the adsorption of MO on a biosorbent based on mango seeds, whereas Yu et al. [13] worked on the adsorption of MO on modified zeolites. Other proposed adsorbents include date palm ash-MgAl-layered double hydroxide composite, surfactant-modified clay [14], and polypyrrole-based graphene oxide [10]. Owing to the inherent drawbacks in the adsorption performance associated with each adsorbent, no unitary adsorbent has been reported to effectively sequester all of the different classes of contaminants. This necessitates the continual search for effective and sustainable adsorbents. Furthermore, two main opportunities for the application of the principles of green chemistry in adsorption science include reduction or reutilization of wastes and the use of less hazardous adsorbent synthesis routes [15]. In this work, an inexpensive regenerated waste-activated carbon is evaluated as an adsorbent, to eliminate methyl orange (MO) by column adsorption in simulated wastewater.

2. Method Experimental

2.1. Collection of Samples and Regeneration of Industrial Activated Carbons. The granular phosphoric acid-activated carbon prepared from coconut husks between 800 and 1000°C produced by the Jacobi Company and used in this study comes from the oily water treatment plant of the Dibamba thermal power plant (Littoral-Cameroon). This spent granular activated carbon (SGAC) was initially used to remove the polyaromatic hydrocarbons, alphaolefins, and paraffins contained in the oily water. Before regeneration, the SGAC material was washed several times for 24 h with demineralized water and then dried at 110°C for 24 h in an oven (Memmert B2162385). The regeneration of the activated carbon was performed by physical and chemical means. Regarding the physical regeneration, 35 g of 3 samples of pretreated SGAC were weighed. The first two samples were put into porcelain crucibles and thermally heated at 700 and 900°C at a rate of 10°C/min in the absence of air, respectively, in a furnace (Nabertherm 30–3,000°C). Once the desired temperature was reached, heating was maintained for 30 min. After thermal treatment, the samples were cooled, washed with HCl (hydrochloric acid 0.05N) with a vol/wt ratio of 2 to remove protic pollutants such as polyaromatic hydrocarbons, followed by hot (60°C) deionized water, cooled again, and finally oven-dried at 110°C for 24 h. The resulting samples were labelled CAR700 and CAR900 corresponding to the temperatures. Furthermore, for chemical regeneration, the third sample of previously weighed SGAC was first socked in hexane (at a liquid/solid ratio of 2) and put under agitation for 24 h to remove protic pollutants such as polyalphaolefins and paraffin contained in SGAC. After filtration, thermal treatment was carried out at 400°C and the material obtained was labelled CAR400. Unused activated carbon (CA) from this oily water treatment plant was used as a reference for comparison purposes in this study.

2.2. Characterization of Activated Carbons. The regenerated activated carbons were characterized by X-ray diffraction by using a Bruker X-ray diffractometer (D8 Discovery, US), Fourier transform infrared spectroscopy (IR Nicolet iS5 from Thermo Fisher Scientific) by using the KBr method (between 4000 and 500 cm^{-1} with a resolution of 2 cm^{-1}), and by the iodine index using the CEFIC 1989 method and the AWWA B 600-78 standard [16].

3. Adsorption Experiments

Duplicate adsorption experiments were carried out under a fixed-bed (Figure 1) using glass columns of different internal diameters (5, 7, and 9 mm) filled with activated carbon of mass (0.1 and 0.2 g) and height (0.25 and 0.5 cm), having at the bottom and top cotton to hold the adsorbent. During the process, a solution of methyl orange of known concentration (mg/L) contained in a beaker is pumped using a peristaltic pump (type BT100-1F Hebei, China) to the tank fitted with a regulating valve to control the flow rate, and at the outlet of the column, the filtrate is collected using an effluent collector [17]. The residual MO concentration in the effluent was measured by a UV-visible spectrophotometer at 465 nm [18].

As the MO solution was introduced into the column, the pollutant was adsorbed depending on certain parameters such as the height of the adsorbent, the flow time, the diameter of the column, and the concentration of the pollutant. By plotting the value of the C_t/C_0 ratio as a function of time, a curve called the "depletion curve" or "breakthrough curve" of active sites of the column was obtained [19]. The adsorption capacity of MO was calculated using the following equations:

$$Q_t = -\frac{F}{1000}\int_{t=0}^{t=t\max} C_{\text{ads}}\mathrm{d}t = \frac{((C_0 - C_t)\times V)}{m_{\text{CA}}}. \quad (1)$$

With

$$C_{\text{ads}} = (C_0 - C_t), \quad (2)$$

q_{ads} is the quantity adsorbed, F is the flow rate, $t_{\max}$ is the total time expressed in (min) required to achieve 90% saturation of the column, Q_t is the adsorption capacity at time t

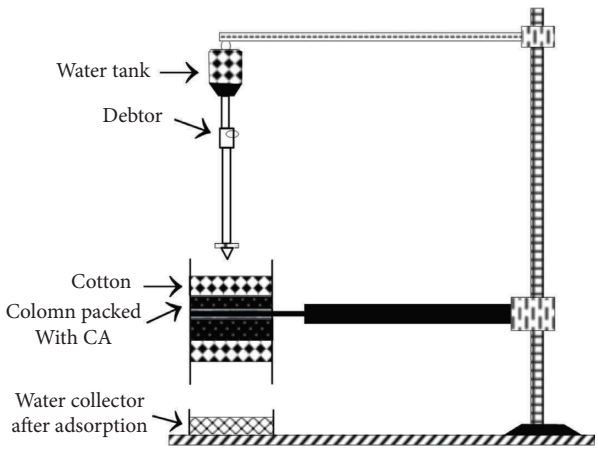

Figure 1: Experimental column adsorption method.

(mg/g), C_0 is the initial dye concentration (mg/L), C_t is the dye concentration at time t (mg/L), V is the volume of the solution (mL), and m_{CA} is the mass of the adsorbent (g).

3.1. Influence of Concentration. Two separate solutions of MO with initial concentrations of 5 and 10 mg/L were passed through a 9 mm diameter column containing 0.2 g of CA, CAR400, CAR700, and CAR900 singly, with a flow rate of 5 mL/min, to evaluate the effect of initial concentration.

3.2. Influence of the Flow Rate. The study on the influence of flow rate was conducted by fixing the diameter of the column at 9mm, the concentration of MO at 10 mg/L, adsorbent dosage at 0.2g, and the flow rates at 2.5 and 5 mL/min adjusted from the pump and the tank flow rate.

3.3. Influence of Column Diameter. The effect of the column diameter on the adsorption of MO was carried out in three columns of 5, 7, and 9 mm diameters, with 0.2 g of each adsorbent. The flow rate was maintained at 5 mL/min with an MO solution of concentration of 10 mg/L.

3.4. Influence of the Height of the Column. The columns of diameter 9 mm were loaded with 0.1 and 0.2 g of the adsorbents. The MO solution with a concentration of 10 mg/L was introduced into the column at a flow rate of 5 mL/min.

4. Results and Discussion

4.1. Adsorbent Characterization

4.1.1. Iodine Number. Table 1 shows the iodine values of the commercial reference-activated carbon CA and the regenerated activated carbons. It can be seen that the different materials have an iodine index greater than 600 mg/g, and according to the specifications of AWWA B 600-78 [20], activated carbons with an iodine index greater than or equal to 600 mg/g can be considered for effluent treatment. Moreover, it is observed that CAR400 presents a microporosity comparable to that of commercial activated carbon (CA) proving that the chemical regeneration was more robust in the restoration of the porosity structure. As for the physically regenerated carbons CAR700 and CAR900, they exhibited poor microporosity compared to CA and CAR400. This is due to the high temperatures that the materials were subjected to during thermal regeneration, which deteriorated the carbon skeleton.

Table 1: Iodine index of the samples.

Samples	CA	CAR400	CAR700	CAR900
Iodine index (mg/g)	1,052	1,045	748	880

4.1.2. XRD Analysis. Figures 2 and Table 2 show, respectively, the diffractograms of CA, CAR400, CAR700, CAR900, and the associated crystalline phases. Based on ASTM (American Society for Testing and Materials) files [21], it is observed that the dome appearing on the diffractograms between 16° and 34.6° is representative of the amorphous phases, with some crystalline phases at 20.98°, 26.84°, and 29.39° corresponding to intercrystalline distances of 4.23 Å, 3.32 Å, and 3.04 Å, respectively, whose peaks are attributable to quartz and calcite present in CAR400, CAR700, and CAR900 materials. However, it should be mentioned that the peak at 29.39° does not appear on the reference-activated carbon CA. Moreover, crystalline phases are observed mainly between 34.60° and 70° on the different materials, and the identification of the different crystalline phases is summarized in Table 2. In sum, it appears that quartz is the major crystalline phase of these diffractograms on the one hand, and on the other hand the regeneration temperatures of the coals (400°C, 700°C, and 900°C) lead to a mineralogical modification with the absence or appearance of crystallization peaks within CA. These results are in agreement with the work of Girgis et al. [22] on the study of XRD diffractograms of activated carbons prepared under various conditions.

4.1.3. FTIR Analysis. Figure 3 shows the FTIR spectra of the different activated carbons recorded between 4000 and 500 cm^{-1}. The weak peaks observed centered around 2912 cm^{-1} and were attributed to the aliphatic C-H elongation bands [23]. The bands observed around 1758 cm^{-1} belong to the C=O bonds of amides and carboxylic acids, whereas the vibration bands around 1540 cm^{-1} are characteristic of the C=C bonds of alkenes and aromatic groups [24]. The bands appearing between 1300 and 1000 cm^{-1} correspond to the stretching of C-O bonds in aromatic groups, carboxylic acids, alcohols, esters, or of the P=O bond in phosphate esters [25]. Bands in the 1000–600 cm^{-1} region correspond to out-of-plane C=C deformation bands in alkenes and C-H in aromatics. Finally, the bands located between 600 and 400 cm^{-1} are attributable to the elongation of C-C bonds [25]. By comparing the FTIR spectra of CAR700 and CAR900 with that of the reference-activated carbon CA, it was found that the absence of the peak at 568 cm^{-1} on the spectrum of the physically regenerated activated carbons was due to the deterioration of these

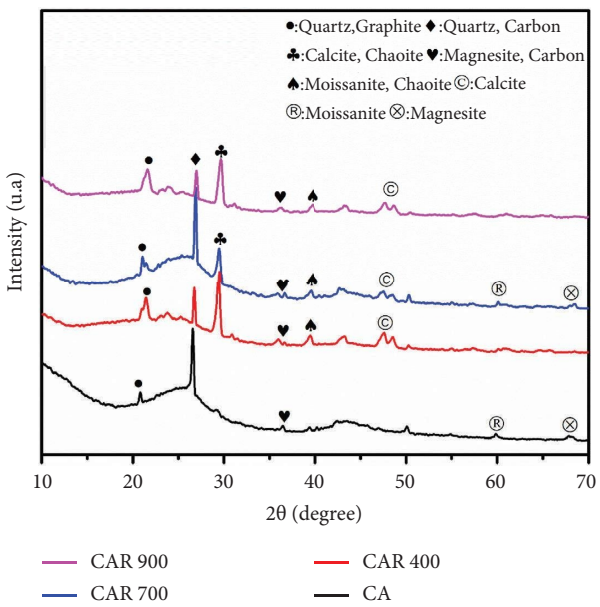

Figure 2: XRD patterns of CA, CAR400, CAR700, and CAR900.

Table 2: Crystalline phases from diffractograms.

2θ (degree)	d_{hkl} (Å)	Crystalline phases
20.98	4.23	Quartz (SiO_2) and graphite (C)
26.84	3.32	Quartz (SiO_2) and carbon (C)
29.38	3.04	Calcite ($CaCO_3$) and chaoite (C)
36.02	2.49	Magnesite ($MgCO_3$) and carbon (C)
36.79	2.44	Moissanite (SiC)
39.78	2.26	Moissanite (SiC) and chaoite (C)
47.63	1.90	Calcite ($CaCO_3$)
50.83	1.80	Quartz (SiO_2) and graphite (C)
60.12	1.53	Calcite ($CaCO_3$) and moissanite (SiC)
68.64	1.36	Magnesite ($MgCO_3$)

bonding sites by the regeneration temperature because some adsorption sites were still occupied by previously adsorbed molecules. As for the CAR400 spectrum, the observed vibrational bands are similar to the CA revealing that the chemical regeneration has restored the initial active sites to that of the unused material despite the appearance of the weak peak at 600 cm^{-1}. In addition, the slight shifts in the vibrational bands observed from 568 to 565 cm^{-1} and from 560 to 558 cm^{-1} are due to restructuring during regeneration. Moreover, the bands of the C=O and C-O groups correlate with the carbonate crystalline phases identified in the XRD section and the different bands thus mentioned will constitute the binding sites with the functions of the MO during the retention process of the latter [26].

4.2. Influence of the Different Parameters

4.2.1. Influence of Concentration. Breakthrough curves postulate that increasing concentration affects bed saturation and breakthrough [27]. Figure 4 and Table 3 show, respectively, the breakthrough curves and experimental data obtained for the two MO concentrations (5 and 10 mg/L) at a constant flow rate of 1.5 mL/min. From these breakthrough curves, it can be seen that increasing the concentration of MO decreases the breakthrough time for all three types of regenerated activated carbons and the commercial ones. The adsorption capacity (Q_t) determined from (1) and (2) reveals that the total MO retained by the carbonaceous materials increased with the concentration from 3.10 to 9.25 mg/g for CA, 2.28 to 2.50 mg/g for CAR400, 3.50 to 5.75 mg/g for CAR700, and 2.25 to 6.75 mg/g for CAR900. The increase in the concentration of MO increased the diffusion of the molecules inside the cavities of the activated carbons. Note that, the quantities of MO adsorbed were greater for the thermally regenerated carbons than for the chemically regenerated carbon (CAR400) despite the underdeveloped porosity structures of CAR700 and CAR900. This shows that the adsorption of MO is not controlled by the microporosity and steric effects.

4.2.2. Influence of the Flow Rate. The flow rate is a critical parameter that affects the performance of the adsorbent [28]. The plots of the breakthrough curve (C_t/C_o) as a function of time (Figure 5) show that when the flow rate is increased, the residence time of the MO molecules decreases in the column hence decreasing the time for MO molecules to diffuse into the adsorbent pores, resulting in a rapid saturation of the adsorption bed and a loss of adsorption efficiency of the carbons [29]. Additionally, an increased flow rate reduces the residence time of MO in the column to allow the system to reach equilibrium, with concomitant desorption of loosely bound MO molecules on the adsorbent surface. The total quantity of methyl orange adsorbed decreased from 8.68 to 3.07 mg/g for CA, 3.63 to 3.01 mg/g for CAR400, 5.75 to 3.68 mg/g for CAR700, and 6.75 to 3.45 mg/g for CAR900 when the flow rate increased from 1.5 to 5 mL/min. Similarly, thermally regenerated carbons (CAR700 and CAR900) exhibited higher removal efficiency than the chemically regenerated carbon, CAR400.

4.2.3. Influence of the Column Diameter. Figure 6 shows the breakthrough curves and the experimental data relating to the influence of the column diameter on the adsorption of MO. From the breakthrough curves, it can be seen that the diameter of the columns influences the performances of the carbons. The column with a diameter of 5 mm has the highest mass transfer zone, which positively influences on the one hand the quantities of MO adsorbed from the CA, CAR400, CAR700, and CAR900 with respective values of 16.90, 9.05, 8.78, and 15.72 mg/g and negatively on the adsorption time because of this small contact surface which results in a faster saturation of 125 min. On the other hand, for columns of diameter 7 and 9 mm, the diameter increases with the contact surface by decreasing the height of the material transfer zone for the same mass adsorbent. Therefore, the 9 mm column has a low adsorption capacity of 9.00, 4.00, 9.00, and 5.78 mg/g, respectively, for CA, CAR400, CAR700, and CAR900 but a long saturation time, which can be justified by a large contact surface. It follows

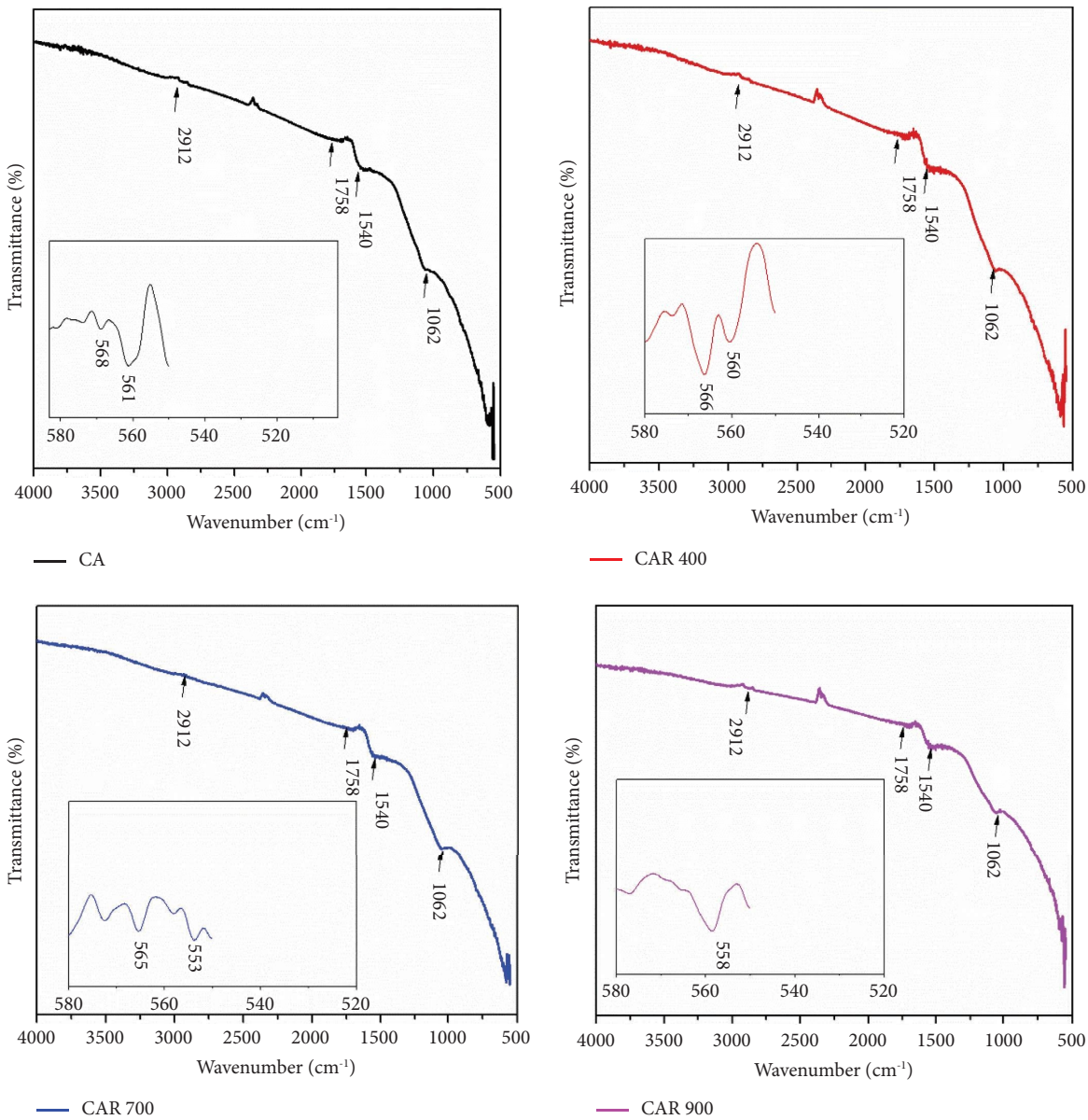

Figure 3: FTIR spectra of regenerated activated carbons.

from these interpretations that the diameter of the column must be proportional to the mass of the adsorbent because the contact surface must be well-defined to facilitate adsorbent-adsorbate interactions to reach equilibrium [30]. This parameter was made contrary to other works to highlight the diameter of the column and not the mass of the adsorbents to study the influences related to the clogging of the column and the speed of exit of the pollutant on the adsorption capacity of these materials.

4.2.4. Influence of the Height of the Column. From the breakthrough curves (Figure 7), it is observed that the quantities of MO adsorbed and the exhaust time increase with the height. Exhaust time is the time when the adsorbent can no longer remove pollutant molecules, and the influent solution leaves the column with no appreciable treatment. The observed increase is due to an increase in the number of active sites of activated carbon following an increase in the number of adsorbent particles. The variation in height is proportional to the breakthrough time; the more the height is increased, the greater the breakthrough time. By increasing the height of the bed, the height of the material transfer zone increases, thus decreasing the rate of solute/solid exchange. It is deduced that the total adsorbed quantities of MO increase with the height passing from 8.45 to 9.10 mg/g for the CA, 0.75 to 2.43 mg/g for the CAR400, 5.00 to 5.70 mg/g for the CAR700, and 5.93 to 6.75 mg/g for the CAR900 for an average saturation time of 170–270 min for the respective heights of 2.5 and 5 mm. This makes it possible to deduce that the higher the height of the column, the greater the quantity adsorbed. Benzekhri obtained

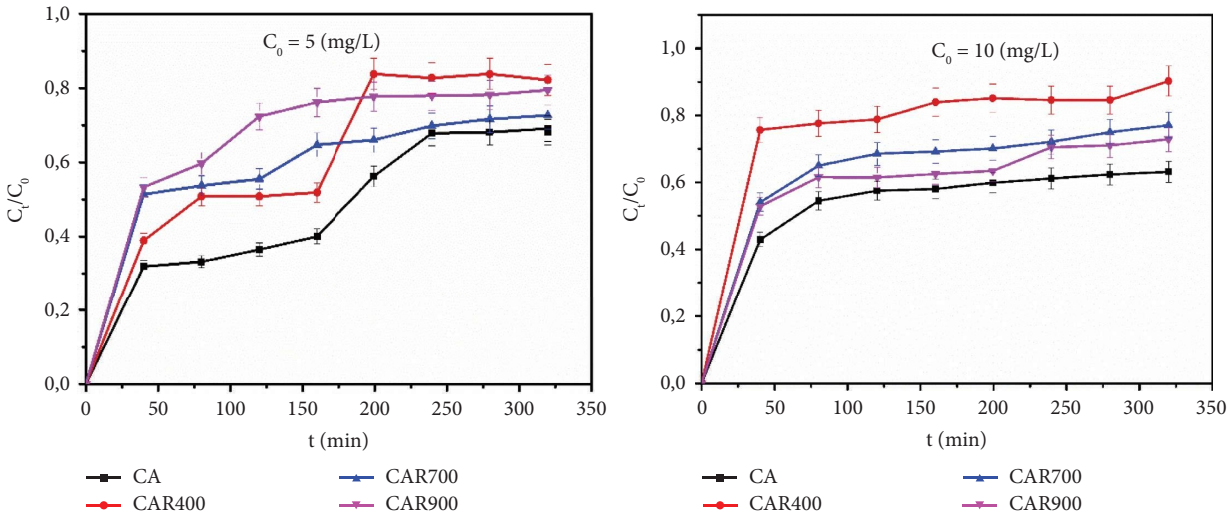

Figure 4: Influence of the concentration on the adsorption process of methyl orange onto different carbons ($F = 1.5\,\text{mL}\cdot\text{min}^{-1}$ and $D = 9\,\text{mm}$).

Table 3: Experimental data on the influence of concentration on the adsorption of methyl orange.

C_o (mg/L)	Materials	Q_t (mg/g)
5	CA	3.10
	CAR400	2.28
	CAR700	3.50
	CAR900	2.25
10	CA	9.25
	CAR400	2.50
	CAR700	5.73
	CAR900	6.75

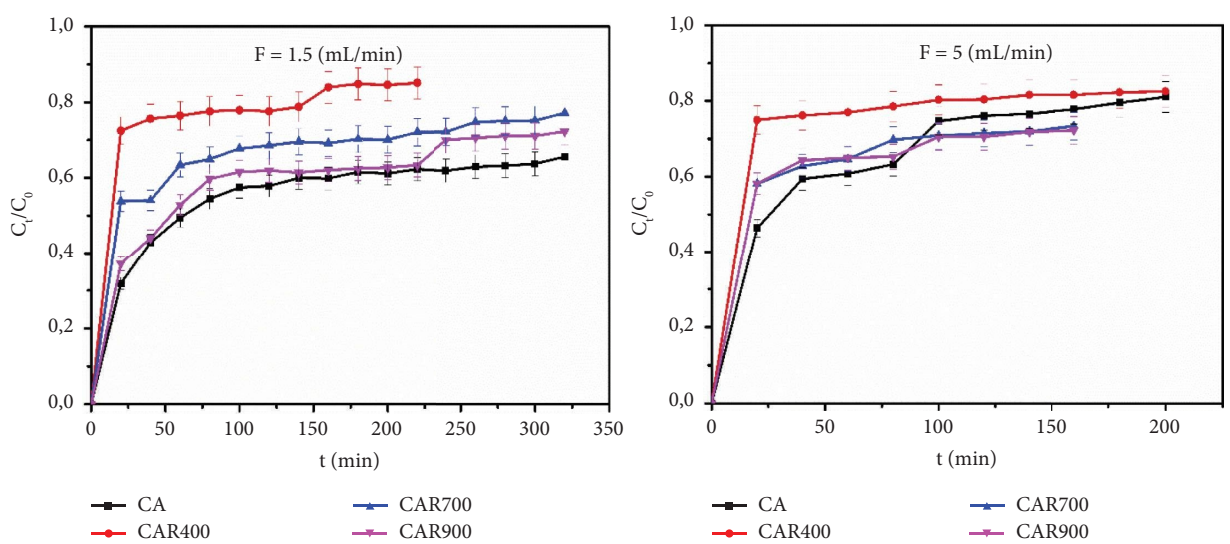

Figure 5: Influence of the flow rate on the adsorption process of methyl orange in contact with the different carbons ($C_0 = 10\,\text{mg}\cdot\text{L}^{-1}$ and $D = 9\,\text{mm}$).

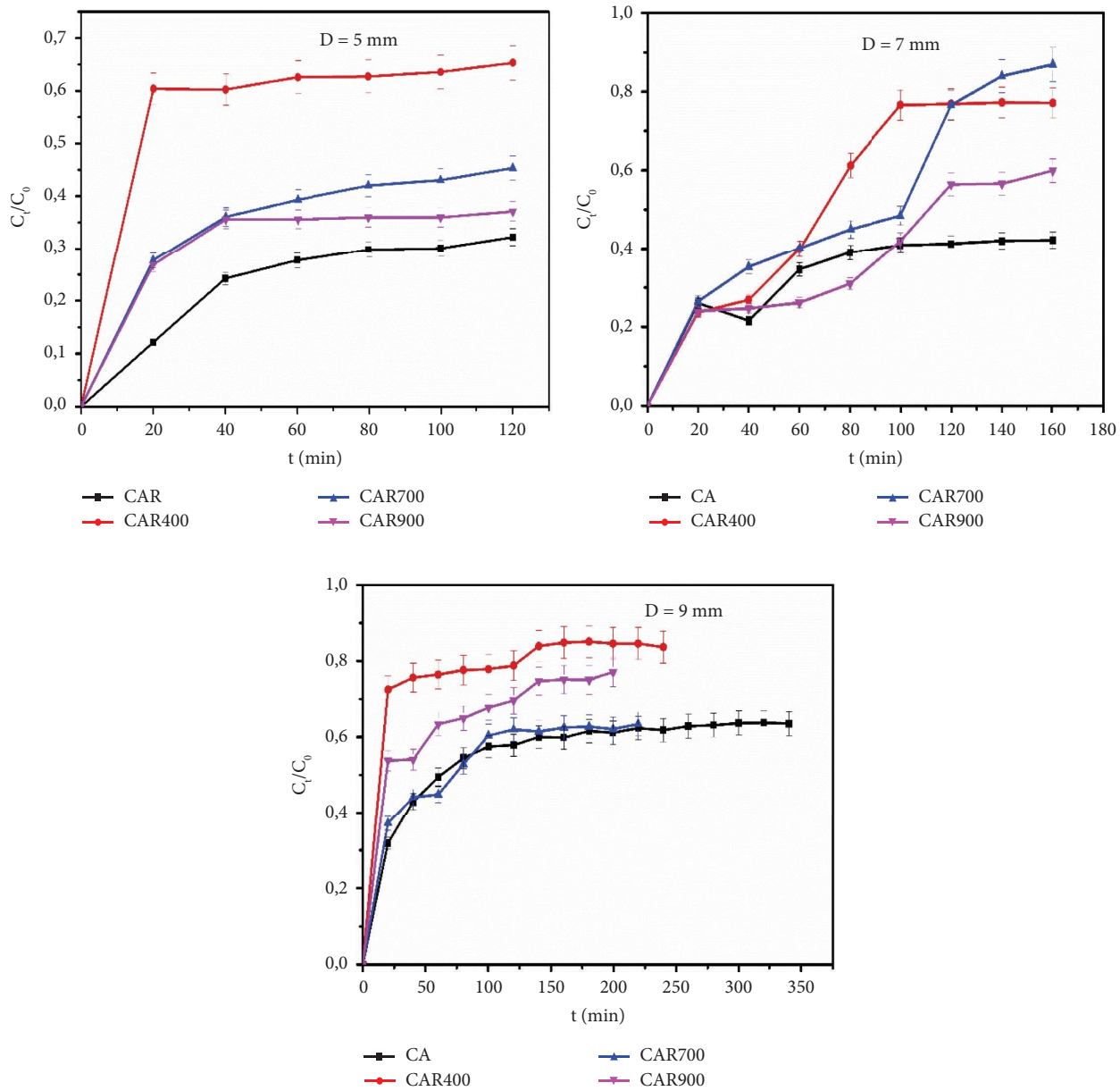

Figure 6: Influence of the diameter on the adsorption process of methyl orange onto different carbons ($C_0 = 10\,\mathrm{mg{\cdot}L^{-1}}$ and $F = 1.5\,\mathrm{mL{\cdot}min^{-1}}$).

similar results for the modelling studies of an adsorption column packed with granulated activated carbon [31].

It emerges from the parameters studied that the optimal conditions are 10 mg/L for the MO concentration, 1.5 mL/min for the flow rate, 5 mm diameter for the column, and 5 mm for the height of the adsorbents in the column. The parameters and capacities of the regenerated activated carbon are close to those of the commercial activated carbon, CA. The thermally regenerated activated carbons were found to be better for column adsorption against MO compared to the chemically regenerated ones. The adsorption efficiency differs depending on the carbon regeneration method. Moreover, the results of FTIR revealed functional differences at the surface of these materials, suggesting that functional group density partly accounts for why the adsorption performances are not identical. In fact, the higher the regeneration temperature, the more the existing surface functions decrease with the regeneration of new functions: the phenomenon of physisorption is observed more than chemisorption. In the literature [32, 33], in fixed-bed studies, physisorption is the predominant phenomenon, which therefore explains why physically regenerated activated carbons have better adsorption capacities and parameters than chemically regenerated carbons.

4.3. Mathematical Models. Various mathematical models have been developed to predict the dynamic behaviour of adsorption through a column and to estimate kinetic parameters. For this study, three mathematical models based

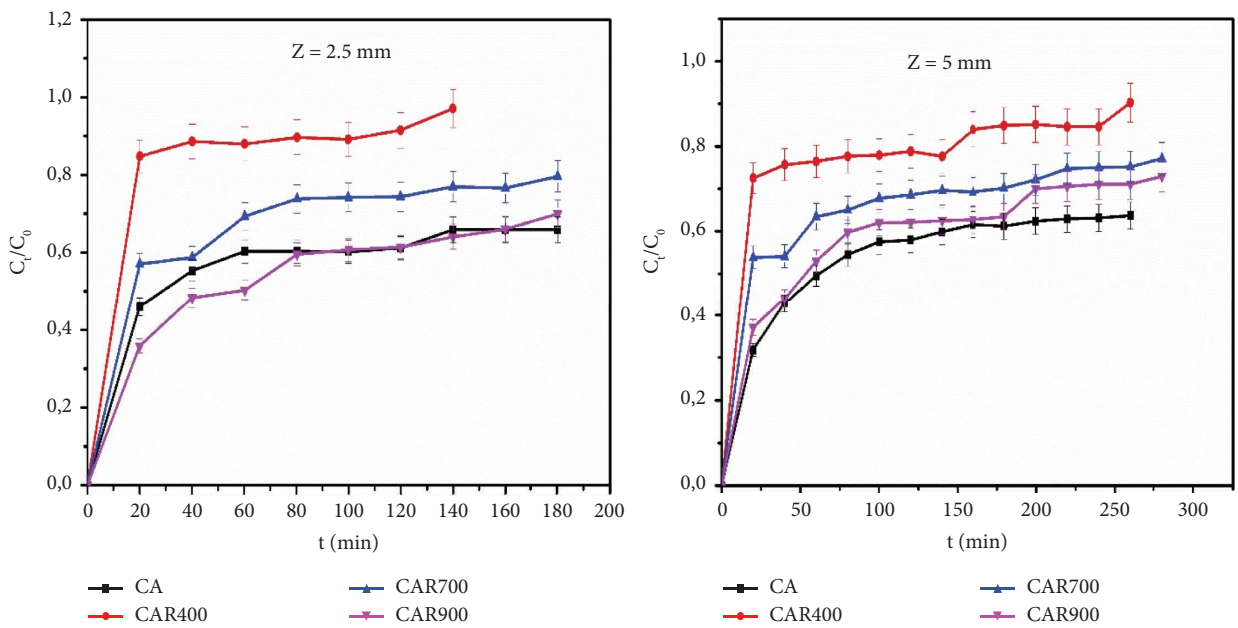

Figure 7: Influence of the variation of the filling height on the adsorption process of MO in contact with the different coals ($C_0 = 10$ mg·L^{-1} and $F = 1.5$ mL·min^{-1}).

on the equations developed by Adams and Bohart [34], Thomas [35], and Yoon and Nelson [36] to describe, predict, and estimate the experimental data obtained from the adsorption studies were carried out on a fixed bed to predict the breakthrough curves.

4.3.1. Thomas Model. The Thomas model is not the most widely used model to describe the sorption process in fixed-bed columns. As explained in the literature review, this model is used for the adsorption of organic, inorganic, and heavy metal compounds. This model is inspired by the Langmuir isotherm and the second-order kinetic model [37, 38]. It states that the flow through the column should be with negligible axial dispersion. It also assumes that adsorption is not limited by the chemical reaction but is rather controlled by mass transfers at the adsorbent/adsorbate [39]. By plotting the curve of (ln $(C_o/C_t - 1)$) against time (t), the parameters of the Thomas model, namely, the constants K_{TH} and q^0 can be determined by using the following equation:

$$\ln\left(\frac{C_0}{C_t} - 1\right) = \frac{K_{TH} q^0 m}{F} - K_{TH} C_0 t, \quad (3)$$

where C_0 is the initial pollutant concentration (mg·L^{-1}), C_t is the effluent concentration at time (t) at the outlet of the column (mg·L^{-1}), m is the bed mass (g), K_{Th} is the Thomas constant (mL·mg^{-1}·min^{-1}), q^0 is the maximum adsorption capacity of the solute on the adsorbent (mg·g^{-1}), F is the column solution feed rate (mL·min^{-1}), and t is the breakthrough time related to the concentration C_t at the outlet of the column (min).

The Thomas model parameters for different column diameters are shown in Table 4. The plots of the Thomas model are displayed in Figure 8. From Table 4, generally, it can be seen that the values of the adsorption capacity (q_0) decreased with an increase in diameter. The rate constants did not follow any logical sequence with the increase in column diameter. Furthermore, from Table 4, we can see that the negative constants and the coefficients of determination $R^2 < 0.90$ are unacceptable to define the mechanisms related to MO retention. Therefore, the Thomas model was inadequate to predict the effect of column diameter on the adsorption dynamics of MO on all the materials.

4.3.2. Bohart and Adams Model. Adams and Bohart [34] established different equations assuming on the one hand that there is an adsorption saturation layer in the dynamic regime on the solid support and on the other hand that the adsorption equilibrium is achieved on each grain and that one can be freed by the reverse desorption reaction [34, 40]. Although this system was built for two-phase gas-solid systems, it also applies very well to a liquid-solid system. The Bohart and Adams model (4) assumes that the adsorption rate is proportional to both the residual capacity of the adsorbent and the concentration of the adsorbate [41].

$$\frac{C_t}{C_0} = \exp\left(\left(K_{AB} C_0 t_b\right) - \left(\frac{K_{AB} N_0 . Z}{v}\right)\right). \quad (4)$$

By linearizing, (5) was obtained as follows:

$$\ln\left(\frac{C_t}{C_0}\right) = K_{AB} C_0 t_b - \frac{K_{AB} N_0 Z}{v}, \quad (5)$$

where t_b stands for the breakthrough time (min), C_0 is the initial concentration (mg·L^{-1}), C_t is the concentration of the solute at equilibrium (mg·L^{-1}), V is the speed in the reactor which is assumed to be empty (cm·min^{-1}), N_0 is the

Table 4: Adsorption parameter of the Thomas model for the different diameters of the columns at a constant flow rate.

Parameters	Materials	D (mm)	K_{TH} (mL·mg^{-1}·min^{-1})	q_o (mg·g^{-1})	R^2
$C_o = 10$ mg·L^{-1} $F = 1.5$ mL·min^{-1}	CA	5	0.001020	13,275.73	0.63
	CAR400		0.000210	−12,907.14	0.91
	CAR700		0.000690	10,263.04	0.83
	CAR900		0.000350	19,097.14	0.43
	CA	7	0.000920	10,858.69	0.71
	CAR400		0.002760	51,24.46	0.94
	CAR700		0.001840	5,995.10	0.80
	CAR900		0.001380	9,028.86	0.85
	CA	9	0.001050	5,578.57	0.86
	CAR400		0.000310	−23,383.06	0.89
	CAR700		0.000105	5,207.86	0.96
	CAR900		0.000740	91.22	0.90

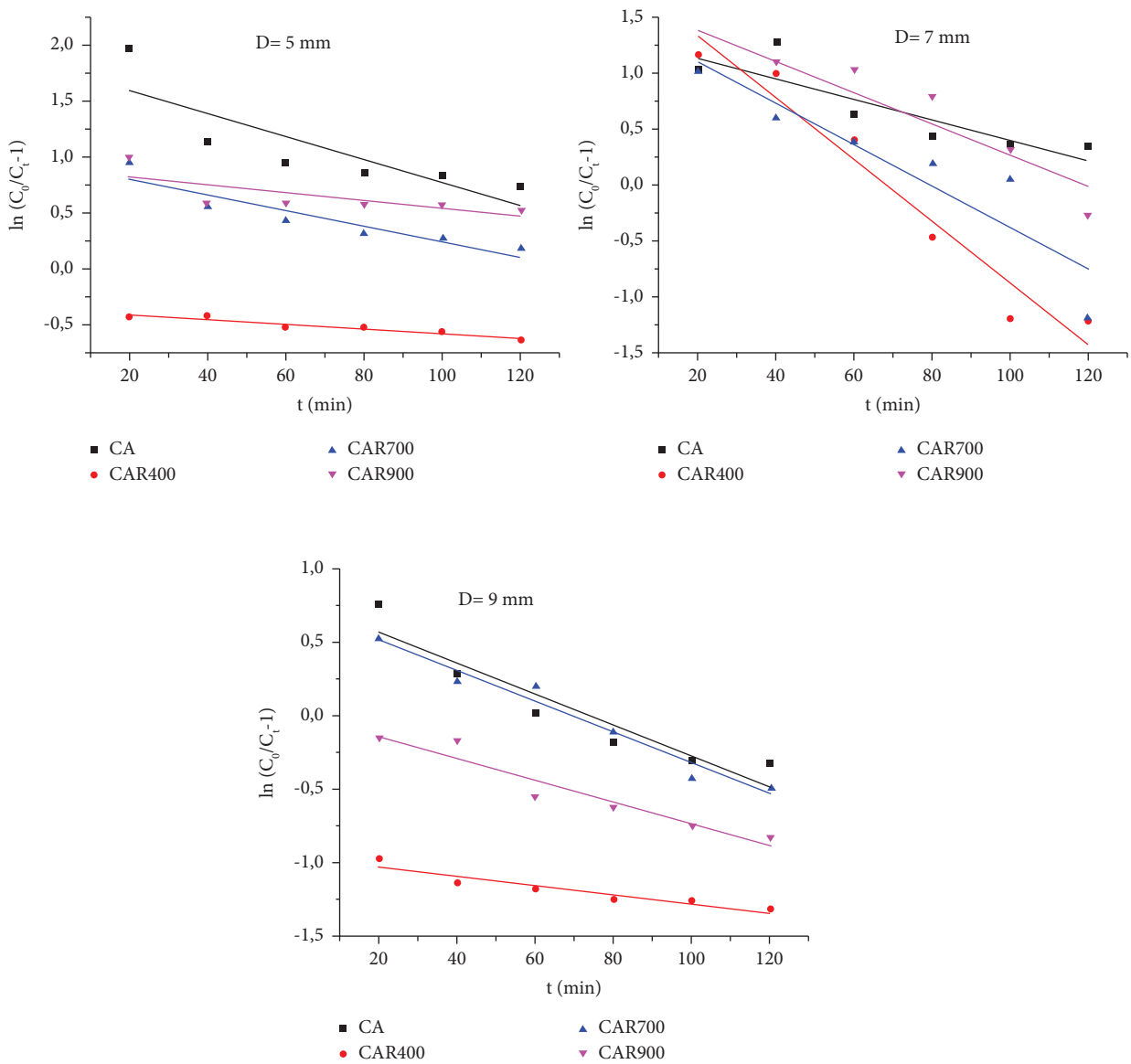

Figure 8: Variation of ln $(C_o/C_t - 1)$ as a function of time for the different diameters.

Table 5: Bohart–Adams' adsorption parameters for different concentrations and the Nelson–Yoon's model for the different filling heights.

Model Bohart–Adams	Materials	C_o (mg·L^{-1})	K_{ab} (mL·mg^{-1}·min^{-1})	N_o (mg·L^{-1})	R^2
	CA	5	0.00032	10,976.72	0.95
	CAR400		0.00076	6,722.89	0.82
	CAR700		0.00032	10,980.64	0.93
$F = 1.5$ mL·min^{-1}	CAR900		0.00040	7,608.99	0.80
$D = 9$ mm	CA	10	0.00015	22,586.77	0.65
	CAR400		0.00006	23,765.20	0.87
	CAR700		0.00012	22,801.53	0.66
	CAR900		0.00011	27,242.98	0.75
Model Nelson–Yoon	**Materials**	**Z (mm)**	**K_{YN} (min^{-1})**	**τ (min)**	**R^2**
	CA	2.5	0.0052	14.05	0.60
	CAR400		0.0052	−327.59	0.75
	CAR700		0.0089	−16.15	0.81
$C_o = 10$ mg·L^{-1}	CAR900		0.0102	59.20	0.84
$F = 1.5$ mL·min^{-1}	CA	5	0.0105	74.38	0.83
	CAR400		0.0031	−311.77	0.68
	CAR700		0.0070	−1.05	0.87
	CAR900		0.0108	58.83	0.82

saturation concentration (model-predicted effluent concentration) (mg·L^{-1}), Z is the bed height (cm), and K_{AB} is the Adams–Bohart constant (L·mg^{-1}·min^{-1}).

Table 5 groups together the adsorption parameters obtained from representative curves (Figure 9) at the two initial concentrations $C_0 = 5$ and 10 mg·L^{-1}. According to the results in Table 5, as the inlet concentration increases, the saturation concentration (N_0) of the methyl orange bed increases and the rate constant (K_{AB}) decreases. When the initial concentration of C_0 is increased, the limited active sites of adsorbent particles become incapable of embedding all the MO molecules in their pores resulting in a higher N_0. These results due to the increase of N_0 and K_{AB} according to the concentration are partially observed in the CAR900 material. It is noted that these observations are in agreement with the results obtained during the modelling studies of an adsorption column packed with granulated activated carbon as cited above [31]. The majority of the correlation coefficients R^2 are greater than 0.8 and are considered a good fitting. Conformity to this model indicates that the surface diffusion is the rate-determining step of the adsorption process. Given the widely varied R^2 values, the model of Bohart and Adams unsatisfactorily describes the breakthrough curves of MO on the materials studied. Furthermore, this model is only applicable to the initial region of the curve ($C_t/C_0 < 0.1$).

4.3.3. Nelson–Yoon Model. This model assumes that the rate of decrease in probable adsorption for each pollutant molecule is proportional to the breakthrough of the adsorbent [42]. The Yoon–Nelson model is just a modified form of the Thomas equation. It is applied to determine the values of the time (τ) corresponding to the adsorption of 50% of the pollutant.

$$\ln\left(\frac{C_t}{C_0 - C_t}\right) = K_{YN}t - \tau K_{YN}, \quad (6)$$

where C_0 is the initial pollutant concentration (mg·L^{-1}), C_t is the concentration of the pollutant at the outlet of the column and at time t (mg·L^{-1}), K_{YN} is Yoon–Nelson's constant (min^{-1}), and τ is the time corresponding to the adsorption of 50% adsorbent (min).

The representative plots (Figure 10) describe the abovementioned adsorption parameters, and the results of the experimental values obtained from the Nelson–Yoon model are shown in Table 5. From Table 5, the negative τ values, which bear no physical meaning, with relatively low R^2 values for non-negative constants attest that the data predicted by the Nelson–Yoon model are impractical. This suggests the inadequacy of the model to predict the experimental data or is attributable to the inherent errors associated with the linearization of nonlinear equations [43]. Given these findings, the Nelson–Yoon model does not allow us to accurately compare MO adsorption curves on regenerated activated carbon.

The study of the adsorption kinetics of CA has shown that Thomas's models and Nelson–Yoon's models describe a large part of the adsorption of these breakthrough curves as well. The CA was used in this work as a reference carbon.

The study of the adsorption kinetics on physically regenerated activated carbon, CAR700 and CAR900 also revealed that the Thomas and Bohart–Adams models describe part of the breakthrough curves of these carbons but a difference in the adsorption process with that of CA is observed. This discrepancy is justified by the results of FTIR with the regeneration of new C-H functions characterized by the appearance of new mineral phases of calcite, carbon, chaoite, and magnesite, described by XRD, thus highlighting new sites favorable to solid-liquid interactions.

Regarding the study of the adsorption kinetics on chemically regenerated carbon at 400°C, we note that only the Bohart–Adams model describes part of the curves of perforations on this material unlike those regenerated by physical means.

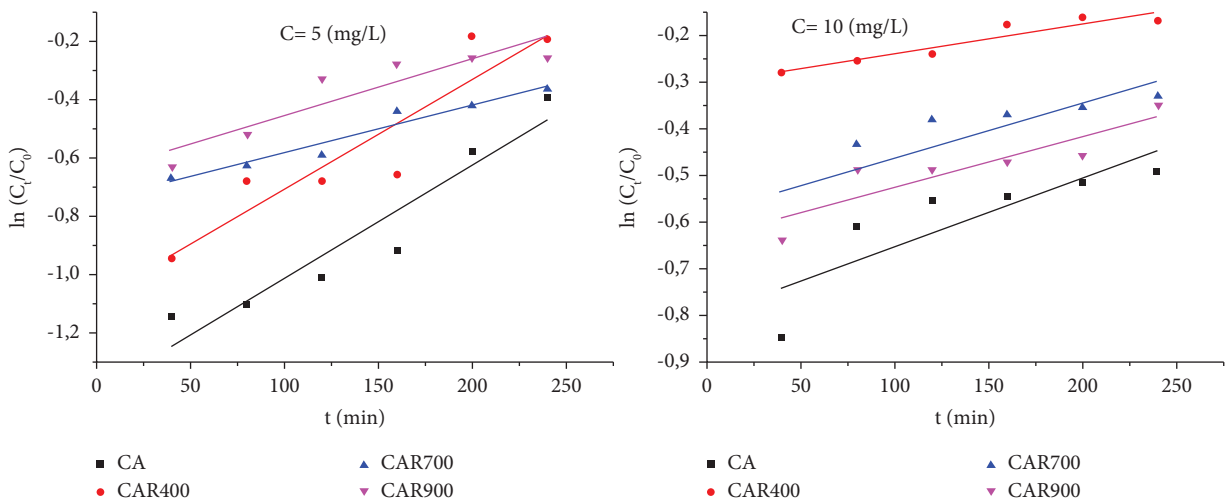

Figure 9: Variation of ln (C_t/C_o) as a function of time at different initial concentrations.

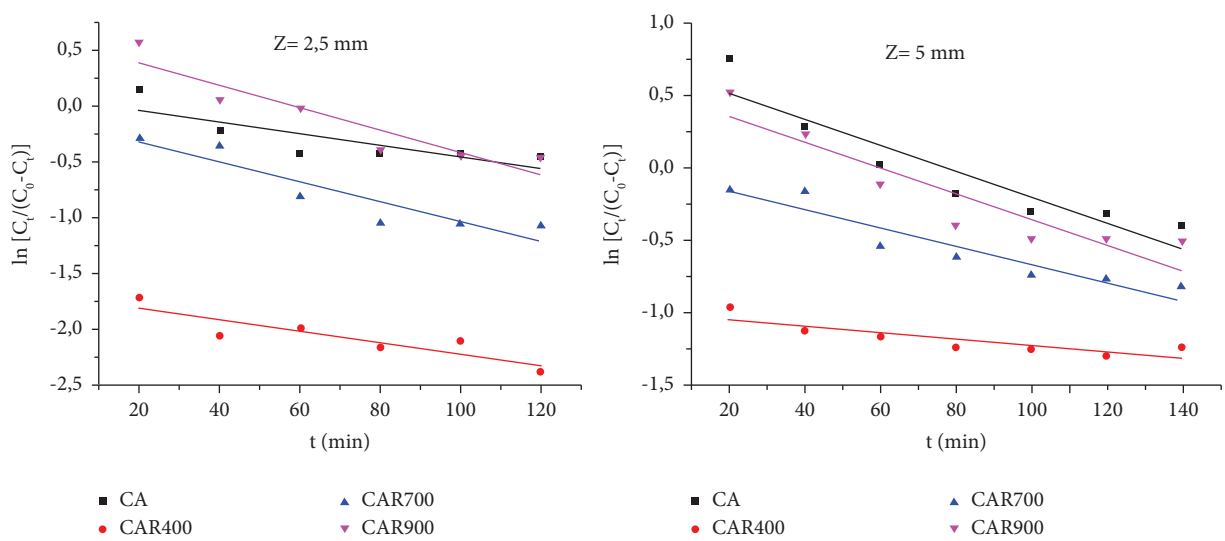

Figure 10: Variation of ln $(C_t/(C_o - C_t))$ as a function of time for the different heights.

5. Comparison of Bed Capacity with Other Adsorbents

From the results obtained from adsorption on the column and in batch mode (Table 6), it is observed that the quantities of MO adsorbed are much more higher in a column for all the carbons than in a batch mode, except for CAR400. In addition, the removal of MO in the column was more suitable for physically regenerated carbons than for chemically regenerated carbons. The CAR900 exhibited the best adsorption capacity (15.72 mg/g), and when compared with other adsorbents in the literature, the adsorption characteristics of CAR900 are still appreciable, given the regeneration. In addition, the physical regeneration of CA is positioned as an alternative for the recovery of waste from the treatment of industrial effluents.

6. Adsorption Mechanisms

Figure 11 highlights the different mechanisms at the CAR-MO interface. The MO retention mechanisms include electrostatic attractive interactions between the sulfonate groups of the MO and the water molecule present on the surface of electrically charged coals behaving like dipoles and (π-π) and (n-π) interactions between the MO and the aromatic and hydroxyl groups of the carbons and the

Table 6: Comparison of the results of the equilibrium adsorption capacity of MO by the materials studied (a) in batch and column mode and (b) with other results from the literature.

(a) Adsorption capacities at equilibrium time

			Column adsorption (this work)	Batch mode [44]
	C_o (mg/L)	m (g)	Q_{exp} (mg/g)	Q_{exp} (mg/g)
CA	10	0.2	9.25	4.87
CAR400	10	0.2	2.50	4.24
CAR700	10	0.2	5.73	3.99
CAR900	10	0.2	6.75	1.59

(b) Comparison with other work on MO

	C_o (mg/L)	Z (cm)	F (mL/min)	Q_{exp} (mg/g)	References
Surfactant-modified chitosan-clinoptilolite composite	100	1.4	7.5	32.09	[45]
Polypyrrole-based activated carbon	30	0.7	1.1	69.1	[10]
Iron-based metal-organic framework	15	1.5	270	21.6	[46]
Natural Garmak clay	100	10.5	5	8.92	[47]
CA	10	1.1	1.5	16.90	This work
CAR400	10	1.1	1.5	9.05	This work
CAR700	10	1.1	1.5	8.78	This work
CAR900	10	1.1	1.5	15.72	This work

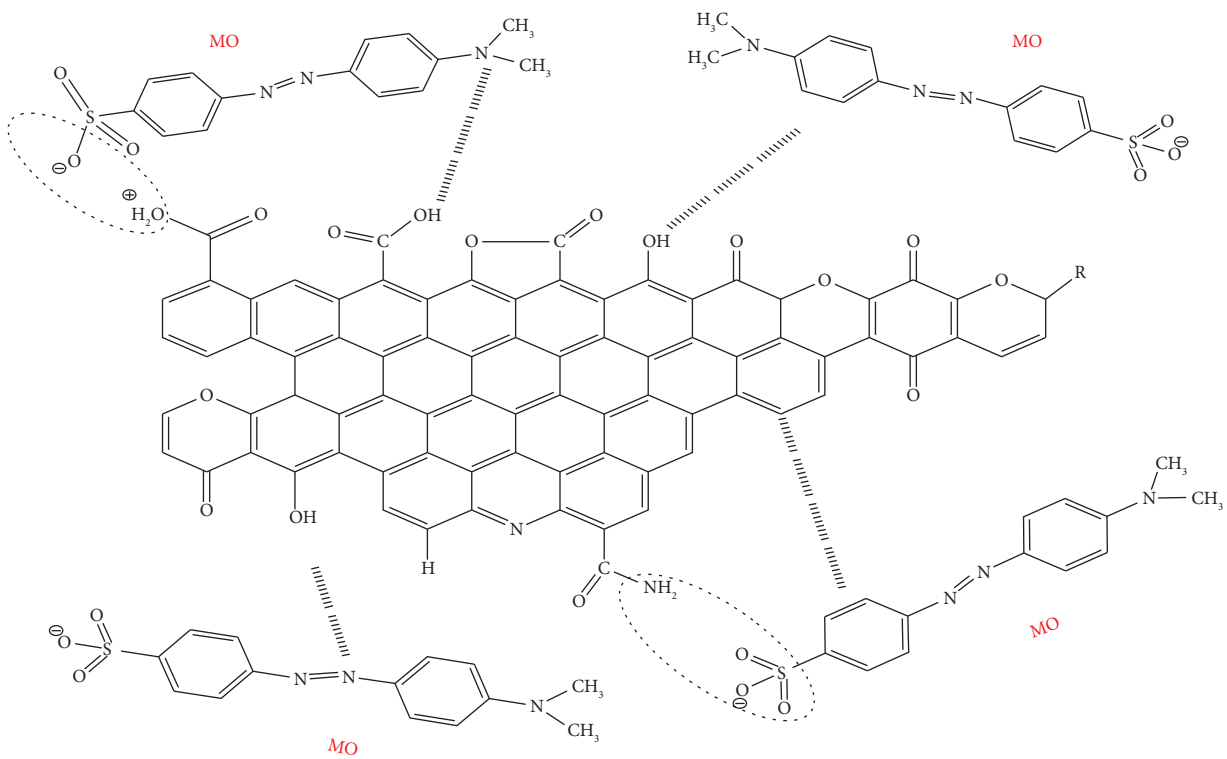

Figure 11: Mechanism highlighting the different chemical bonds likely to occur during the adsorption of MO.

formation of hydrogen bonding. Similar interactions have been observed for the adsorption of other dyes onto activated carbon [8]. In addition, physisorption is predominant during the fixation of MO on CAR in a continuous regime, as alluded by mathematical models.

7. Conclusion

This work evaluated the adsorption performance of chemically and thermally regenerated activated carbons to determine the best valorization approach for waste carbons. The physicochemical characterizations showed that the CAR400 chemically activated carbon has functional groups and a microporosity (1045 mg/g) comparable to that of the reference commercial (CA) activated carbon (1052 mg/g), unlike the physically regenerated carbons. Fixed-bed methyl orange adsorption experiments revealed that the retention capacities of these materials are independent of the porosity structure. The CAR900 material and CA had comparable adsorption capacities of 15.72 and 16.90 mg/g, respectively. The breakthrough curves were best described by the Thomas model than the Bohart–Adams and Yoon–Nelson's models. Thomas's model depicted that an increase in column diameter resulted in a decrease in the maximum adsorption capacity (q_o). The physical/thermal regeneration of activated carbons is shown to be more suitable for the recovery of spent granular activated carbon (SGAC) for the removal of dyes from wastewater in a fixed-bed system.

Data Availability

The data used to support the findings of this study are included within the article.

Conflicts of Interest

The authors declare that they have no conflicts of interest.

Authors' Contributions

Hermann Tamaguelon Dzoujo and David Daniel Joh Dina validated the study, proposed the methodology, reviewed and edited the study, visualized the study, and wrote the original draft. Idriss Kamdem Taquieteu, Hermann Tamaguelon Dzoujo, and Victor Odhiambo Shikuku conceptualised the study, proposed the methodology, investigated the study, wrote the original draft, and collected the resources. Hermann Tamaguelon Dzoujo, Victor Odhiambo Shikuku, David Daniel Joh Dina, Charles Banenzoué, and Idriss Kamdem Taquieteu reviewed, edited, and validated the study. David Daniel Joh Dina, Hermann Tamaguelon Dzoujo, and Charles Banenzoué collected the resources and supervised the study.

References

[1] K. Badvi and V. Javanbakht, "Enhanced photocatalytic degradation of dye contaminants with TiO2 immobilized on ZSM-5 zeolite modified with nickel nanoparticles," *Journal of Cleaner Production*, vol. 280, Article ID 124518, 2021.

[2] G. Derouich, S. Alami Younssi, J. Bennazha, J. A. Cody, M. Ouammou, and M. El Rhazi, "Development of low-cost polypyrrole/sintered pozzolan ultrafiltration membrane and its highly efficient performance for Congo red dye removal," *Journal of Environmental Chemical Engineering*, vol. 8, no. 3, Article ID 103809, 2020.

[3] R. Han, Y. Wang, W. Yu, W. Zou, J. Shi, and H. Liu, "Biosorption of methylene blue from aqueous solution by rice husk in a fixed-bed column," *Journal-of-hazardous-Materials*, vol. 141, no. 3, pp. 713–718, 2007.

[4] P. Waranusantigul, P. Pokethitiyook, M. Kruatrachue, and E. S. Upatham, "Kinetics of basic dye (methylene blue) biosorption by giant duckweed (Spirodela polyrrhiza)," *Environmental Pollution*, vol. 125, no. 3, pp. 385–392, 2003.

[5] A. C. Mecha and M. N. Chollom, "Photocatalytic ozonation of wastewater: a review," *Environmental Chemistry Letters*, vol. 18, no. 5, pp. 1491–1507, 2020.

[6] E. Ngeno, E. Mbuci, M. Necibi et al., "Sustainable reutilization of waste materials as adsorbents for water and wastewater treatment in Africa: recent studies, research gaps, and way forward for emerging economies," *Environmental Advances*, vol. 9, Article ID 100282, 2022.

[7] J. B. Njewa and V. O. Shikuku, "Recent advances and issues in the application of activated carbon for water treatment in Africa: a systematic review (2007–2022)," *Applied Surface Science Advances*, vol. 18, Article ID 100501, 2023.

[8] M. B. Jacques, N. P. Guy, M. L. Jules et al., "Removal of crystal violet by TiO2 loaded alkali-activated carbon hybrid material from Raphia farinifera fruit kernels: surface chemistry, parameters and mechanisms," *Biomass Conversion and Biorefinery*, 2023.

[9] H. T. Dzoujo, V. O. Shikuku, S. Tome et al., "Synthesis of pozzolan and sugarcane bagasse derived geopolymer-biochar composites for methylene blue sequestration from aqueous medium," *Journal of Environmental Management*, vol. 318, Article ID 115533, 2022.

[10] A. A. Alghamdi, W. S. Saeed, M. S. Almutairi, F. A. Alharthi, T. Aouak, and A. Al-kahtani, "Adsorption of azo dye methyl orange from aqueous," *Molecules*, vol. 24, 2019.

[11] K. Akansha, D. Chakraborty, and S. G. Sachan, "Decolorization and degradation of methyl orange by Bacillus stratosphericus SCA1007," *Biocatalysis and Agricultural Biotechnology*, vol. 18, Article ID 101044, 2019.

[12] A. M. A. O Khelifi, I. Mehrez, M. Younsi, and M. Nacef, "Adsorption du méthylorange sur un biosorbant à base de noyaux de mangue methyl orange adsorption on biosorbent derived from mango seed kernels," *Larhyss Journal*, vol. 36, pp. 145–156, 2018.

[13] X. Yu, H. Lü, G. Zhou, L. Zhou, and Y. Zhang, "Absorption of methyl orange by modified fly zeolites," *Advanced Materials Research*, vol. 476-478, pp. 1365–1369, 2012.

[14] D. Chen, J. Chen, X. Luan, H. Ji, and Z. Xia, "Characterization of anion – cationic surfactants modified montmorillonite and its application for the removal of methyl orange," *Chemical Engineering Journal*, vol. 171, no. 3, pp. 1150–1158, 2011.

[15] E. K. Owino, V. O. Shikuku, W. N. Nyairo, C. O. Kowenje, and B. Otieno, "Valorization of solid waste incinerator fly ash by geopolymer production for removal of anionic bromocresol green dye from water: kinetics, isotherms and thermodynamics studies," *Sustainable Chemistry for the Environment*, vol. 3, Article ID 100026, 2023.

[16] A. Diop, M. Faye, D. Diedhiou, and C. G. M. Diop, "Effect of the nature of the activating agent on the performance of activated carbons prepared from neem seed hulls

(Azadirachta indica A. Juss): application to the elimination of methylene blue in aqueous solution," *Journal of Materials and Environmental Science*, vol. 13, no. 11, pp. 1142–1153, 2022.

[17] U. Kumari, S. Biswas, and B. C. Meikap, "Defluoridation characteristics of a novel adsorbent developed from ferroalloy electric arc furnace slag: batch, column study and treatment of industrial wastewater," *Environmental Technology and Innovation*, vol. 18, Article ID 100782, 2020.

[18] E. Malkoc and Y. Nuhoglu, "Removal of Ni (II) ions from aqueous solutions using waste of tea factory: adsorption on a fixed-bed column," *Journal of Hazardous Materials*, vol. 135, no. 1-3, pp. 328–336, 2006.

[19] C. P. Dwivedi, J. N. Sahu, C. R. Mohanty, B. R. Mohan, and B. C. Meikap, "Column performance of granular activated carbon packed bed for Pb (II) removal," *Journal of Hazardous Materials*, vol. 156, no. 1-3, pp. 596–603, 2008.

[20] B. M. Van Vliet, "Regeneration of activated carbon," *Journal of the Southern African Institute of Mining and Metallurgy*, vol. 91, no. 5, pp. 159–167, 1991.

[21] S. Gates-Rector and T. Blanton, "The Powder Diffraction File: a quality materials characterization database," *Powder Diffraction*, vol. 34, no. 4, pp. 352–360, 2019.

[22] B. S. Girgis, Y. M. Temerk, M. M. Gadelrab, and I. D. Abdullah, "X-Ray diffraction patterns of activated carbons prepared under various conditions," *Carbon letters*, vol. 8, no. 2, pp. 95–100, 2007.

[23] A. Kumar and H. M. Jena, "Preparation and characterization of high surface area activated carbon from Fox nut (Euryale ferox) shell by chemical activation with H3PO4," *Results in Physics*, vol. 6, pp. 651–658, 2016.

[24] D. Mohan, H. Kumar, A. Sarswat, M. Alexandre-franco, and C. U. Pittman, "Cadmium and lead remediation using magnetic oak wood and oak bark fast pyrolysis bio-chars," *Chemical Engineering Journal*, vol. 236, pp. 513–528, 2014.

[25] R. Hoseinzadeh Hesas, A. Arami-Niya, W. M. A. Wan Daud, and J. N. Sahu, "Preparation and characterization of activated carbon from apple waste by microwave-assisted phosphoric acid activation: application in methylene blue adsorption," *Bioresources*, vol. 8, no. 2, pp. 2950–2966, 2013.

[26] S. K. Dutta, M. K. Amin, J. Ahmed, M. Elias, and M. Mahiuddin, "Removal of toxic methyl orange by a cost-free and eco-friendly adsorbent: Mechanism, phytotoxicity, thermodynamics, and kinetics," *South African Journal of Chemical Engineering*, vol. 40, pp. 195–208, 2022.

[27] W. Zhang, L. Dong, H. Yan et al., "Removal of methylene blue from aqueous solutions by straw based adsorbent in a fixed-bed column ☆," *Chemical Engineering Journal*, vol. 173, no. 2, pp. 429–436, 2011.

[28] R. Han, J. Zhang, W. Zou, H. Xiao, J. Shi, and H. Liu, "Biosorption of copper (II) and lead (II) from aqueous solution by chaff in a fixed-bed column," *Journal of Hazardous Materials*, vol. 133, no. 1-3, pp. 262–268, 2006.

[29] M. A. E. de Franco, C. B. de Carvalho, M. M. Bonetto, R. de Pelegrini Soares, and L. A. Féris, "Diclofenac removal from water by adsorption using activated carbon in batch mode and fixed-bed column: isotherms, thermodynamic study and breakthrough curves modeling," *Journal of Cleaner Production*, vol. 181, pp. 145–154, 2018.

[30] I. Bencheikh, K. Azoulay, J. Mabrouki, S. El Hajjaji, A. Moufti, and N. Labjar, "The use and the performance of chemically treated artichoke leaves for textile industrial effluents treatment," *Chemical Data Collections*, vol. 31, Article ID 100597, 2021.

[31] B. B. Mokhtar, "Modélisation d ' une colonne d ' adsorption garnie de charbon actif granulé," Abdel Hamid Ben Badis-mostagnem, Mostaganem, Algeria, Thèse de doctorat, 2018.

[32] R. M. Barrer, *Zeolites and Cloy Minerals Adsorbents and Molecular Sieves*, Academic Press, Cambridge, MA, USA, 2016.

[33] D. W. Breck, *Zeolites and Molecular Sieves: Structure, and Use*, John Wiley and Sons, Hoboken, NJ, USA, 1973.

[34] E. Q. Adams and G. S. Bohart, "Some aspects of the behavior of charcoal with respect to chlorine," *Journal of the American Chemical Society*, vol. 42, pp. 523–544, 1920.

[35] H. Thomas, "Heterogeneous ion exchange in a flowing system," *Journal of the American Chemical Society*, vol. 66, pp. 1664–1666, 1994.

[36] Y. Yoon and J. Nelson, "A theoretical model for respirator cartridge service life," *American Industrial Hygiene Association Journal*, vol. 45, pp. 509–516, 1984.

[37] T. Hong, L. Wei, K. Cui et al., "Adsorption performance of volatile organic compounds on activated carbon fibers in a fixed bed column," *Journal of Environmental Chemical Engineering*, vol. 9, no. 6, Article ID 106347, 2021.

[38] N. Dammak, N. Fakhfakh, S. Fourmentin, and M. Benzina, "Natural clay as raw and modified material for efficient o-xylene abatement," *Journal of Environmental Chemical Engineering*, vol. 1, no. 4, pp. 667–675, 2013.

[39] M. Auta and B. H. Hameed, "Acid modified local clay beads as effective low-cost adsorbent for dynamic adsorption of methylene blue," *Journal of Industrial and Engineering Chemistry*, vol. 19, no. 4, pp. 1153–1161, 2013.

[40] M. Sahel and F. Dusart, "Revue des sciences de l ' eau Journal of Water Science Adsorption dynamique en phase liquide sur charbon actif: comparaison et simplification de différents modèles Dynamic adsorption on activated carbon in the liquid phase comparison and simplification o," *Revue des sciences de l'eau Journal of Water Science*, vol. 6, no. 1, pp. 63–80, 2023.

[41] R. Brion-Roby, "Traitement d'eaux contaminées par l'arsenic et par le molybdène à partir d'un nouvel adsorbant de chitosane," *Université Du Québec À Rimouski*, vol. 53, no. 9, pp. 1689–1699, 2018.

[42] Y. H. E. E. Yoon and J. H. Nelson, "Application of gas adsorption kinetics I. A theoretical model for respirator cartridge service life," *American Industrial Hygiene Association Journal*, vol. 45, no. 8, pp. 509–516, 2010.

[43] J. Tagbo, N. Ositadinma, C. Iheanacho, C. Chiedozie, and C. E. Onu, "Linear and nonlinear kinetics analysis and adsorption characteristics of packed bed column for phenol removal using rice husk- activated carbon," *Applied Water Science*, vol. 12, no. 5, pp. 1–16, 2022.

[44] M. Conde Asseng, H. T. Dzoujo, D. D. Joh Dina, M. A. Etoh, A. N. Tchakounte, and J. N. Nsami, "Batch studies for the removal of a hazardous azo dye methyl orange from water through adsorption on regenerated activated carbons," *Journal of Materials Science and Engineering B*, vol. 10, no. 3, pp. 109–123, 2020.

[45] M. Babazadeh, H. Abolghasemi, M. Esmaeili, and A. Ehsani, "Comprehensive batch and continuous methyl orange removal studies using surfactant modified chitosan-clinoptilolite composite," *Separation and Purification Technology*, vol. 267, no. January, Article ID 118601, 2021.

[46] A. K. R. Sabouni and M. H. Al Sayah, "Adsorption potentials of iron- based metal– organic framework for methyl orange removal: batch and fixed- bed column studies," *International journal of Environmental Science and Technology*, Article ID 0123456789, 2021.

[47] K. A. Babakr and B. K. Aziz, "Adsorptive removal of methyl orange from aqueous solutions with natural Garmak clay as cheap and efficient adsorbent in batch and continuous systems," *Journal of Zankoy Sulaimani*, vol. 2, pp. 183–200, 2019.